Additively manufactured space-filling meta-implants

Kolken, H. M.A.; de Jonge, C. P.; van der Sloten, T.; Garcia, A. Fontecha; Pouran, B.; Willemsen, K.; Weinans, H.; Zadpoor, A. A.

DOI
10.1016/j.actbio.2021.02.020

Publication date
2021

Document Version
Final published version

Published in
Acta Biomaterialia

Citation (APA)
Kolken, H. M. A., de Jonge, C. P., van der Sloten, T., Garcia, A. F., Pouran, B., Willemsen, K., Weinans, H., & Zadpoor, A. A. (2021). Additively manufactured space-filling meta-implants. *Acta Biomaterialia*, *125*, 345-357. https://doi.org/10.1016/j.actbio.2021.02.020

Acta Biomaterialia 125 (2021) 345–357

Contents lists available at ScienceDirect

Acta Biomaterialia

journal homepage: www.elsevier.com/locate/actbio

Full length article

Additively manufactured space-filling meta-implants

H.M.A. Kolken[a,*], C.P. de Jonge[a], T. van der Sloten[b], A. Fontecha Garcia[b], B. Pouran[c], K. Willemsen[c], H. Weinans[a,c], A.A. Zadpoor[a]

[a] Department of Biomechanical Engineering, Delft University of Technology, Delft, the Netherlands
[b] 3D Systems – LayerWise NV, Leuven, Belgium
[c] Department of Orthopedics and Department of Rheumatology, University Medical Center Utrecht, Utrecht, the Netherlands

ARTICLE INFO

Article history:
Received 13 November 2020
Revised 10 February 2021
Accepted 14 February 2021
Available online 19 February 2021

Keywords:
Meta-biomaterials
Non-auxetic
Meta-implants
Acetabular cup
Shape-matching

ABSTRACT

The unprecedented properties of meta-biomaterials could pave the way for the development of life-lasting orthopedic implants. Here, we used non-auxetic meta-biomaterials to address the shortcomings of the current treatment options in acetabular revision surgery. Due to the severe bone deficiencies and poor bone quality, it can be very challenging to acquire adequate initial implant stability and long-term fixation. More advanced treatments, such as patient-specific implants, do guarantee the initial stability, but are formidably expensive and may eventually fail due to stress shielding. We, therefore, developed meta-implants furnished with a deformable porous outer layer. Upon implantation, this layer plastically deforms into the defects, thereby improving the initial stability and homogeneously stimulating the surrounding bone. We first studied the space-filling behavior of additively manufactured pure titanium lattices, based on six different unit cells, in a compression test complemented with full-field strain measurements. The diamond, body-centered cubic, and rhombic dodecahedron unit cells were eventually selected for the design of the deformable porous outer layer. Each design came in three different relative density profiles, namely maximum (MAX), functionally graded (FG), and minimum (MIN). After their compression in bone-mimicking molds with simulated acetabular defects, the space-filling behavior of the implants was evaluated using load-displacement curves, micro-CT images, and 3D reconstructions. The meta-implants with an FG diamond infill exhibited the most promising space-filling behavior. However, the required push-in forces exceed the impact forces currently applied in surgery. Future research should, therefore, focus on design optimization, to improve the space-filling behavior and to facilitate the implantation process for orthopedic surgeons.

Statement of significance

Ideally, orthopedic implants would last for the entire lifetime of the patient. Unfortunately, they rarely do. Critically sized defects are a common sight in the revision of acetabular cups, and rather difficult to treat. The permanent deformation of lattice structures can be used to create shape-morphing implants that would fill up the defect site, and thereby restore the physiological loading conditions. Bending-dominated structures were incorporated in the porous outer layer of the space-filling meta-implants for their considerable lateral expansion in response to axial compression. A functionally graded density offered structural integrity at the joint while enhancing the deformability at the bone-implant interface. With the use of a more ductile metal, CP-Ti, these meta-implants could be deformed without strut failure.

1. Introduction

The concept of architected metamaterials has played an important role in the development of materials with advanced functionalities [1–3]. A desired set of mechanical (*e.g.*, elastic modulus, Poisson's ratio), geometrical (*e.g.*, curvature), mass-transport (*e.g.*,

* Corresponding author.
E-mail address: h.m.a.kolken@tudelft.nl (H.M.A. Kolken).

https://doi.org/10.1016/j.actbio.2021.02.020

permeability, diffusivity), and biological properties (*e.g.*, tissue regenerative performance) may be obtained through the rational design of the small-scale architecture of such materials [4]. The term 'meta-biomaterials' may be used to refer to these multi-physics metamaterials when they target biomedical applications to address challenges that are ordinarily impossible to solve [5,6]. For example, a combination of meta-biomaterials with positive and negatives values of the Poisson's ratio has been shown to compress bone-tissue on both sides of a hip stem, thereby improving implant fixation [7].

In this study, we developed deformable meta-implants using non-auxetic meta-biomaterials for the treatment of acetabular bone defects, which are frequently encountered in the revision of total hip replacement (THR) surgeries (Fig. 1A). The acetabular component is involved in more than 50% of such revisions, with the most common cause being aseptic loosening (*i.e.*, the mechanical failure of the bone implant interface) [8–10]. An acetabular revision can be very challenging, due to the moderate to severe bone deficiencies and poor bone quality (Fig. 1A) [11,12]. Several treatment options are available, including structural allografts, (jumbo) non-cemented hemispherical cups, oblong cups, antiprotrusio cages, or Trabecular Metal augments and shells [12–16]. However, many of those procedures have too short of a service life, which is primarily caused by a lack of adequate fixation and loading [12,13]. Surgeons can opt for an additively manufactured (AM) patient-specific acetabular triflange implant, in which three flanges are used to secure numerous screws in the ischium, pubis, and ilium [17]. This results in adequate primary stability, but since all forces will now be transferred through the flanges, a non-physiological loading condition is created. The pressure will primarily be directed at the acetabular rim, which means the bone surrounding the cup, especially the medial wall, will be unloaded, eventually leading to bone resorption (the Wolff's law) [18]. This phenomenon is known as stress shielding and may ultimately lead to implant loosening [19–21]. Furthermore, patient-specific design of such implants increases the costs.

To address both abovementioned shortcomings (*i.e.*, functionality and cost), we designed AM acetabular cups furnished with a deformable porous outer layer. The latter will plastically deform into the defects upon implantation (Fig. 1B). Filling up these defects will improve the initial stability of the implant at the bone-implant interface, by continuously and homogeneously stimulating the bone surrounding the implant (the Wolff's law) [18]. Moreover, the porous outer layer enables bony ingrowth [22], thereby enhancing the secondary fixation of the implant. Finally, given that the outer layer deforms to fill the defect space, there is no need for a patient-specific design and the high costs that are associated with that.

We started by studying the space-filling behaviors of AM lattices based on six different types of non-auxetic unit cells (Fig. 1C). Given that high levels of ductility are needed to achieve such space-filling behaviors, we used commercially pure titanium (CP-Ti) powder [23]. Compression tests were performed to obtain the stress-strain curves for each of the non-auxetic meta-biomaterials, which were used to calculate their quasi-static mechanical properties. Full-field strain measurements were also performed using digital image correlation (DIC) [24], to determine the Poisson's ratio of the structures, which is expected to be correlated with their space-filling behavior. Based on the results of the first step, three unit cell types were chosen for the design of the porous outer layer with three different profiles of relative density, namely maximum (MAX), functionally graded (FG), and minimum (MIN) (Fig. 1D). Then, a total of 27 deformable meta-implants were compressed in bone-mimicking molds with several replicated acetabular defects (Fig. 1E). The space-filling behavior of the meta-implants was evaluated using the load-displacement curves, micro-CT images, and 3D reconstructions.

2. Materials and methods

2.1. Design and manufacturing

2.1.1. Non-auxetic meta-biomaterials

Six different unit cell types were used to design 5 × 5 × 5 unit cell arrays using the additive manufacturing software 3DXpert 13.0 (3D Systems, Leuven, Belgium). They included the diamond (D), rhombic dodecahedron (RD), cube (C), truncated cube (TC), truncated cuboctahedron (TCO), and body-centered cubic (BCC) unit cells (Fig. 1C). All unit cells were chosen because of their positive (and relatively large) Poisson's ratios and previous consideration in meta-biomaterials [3,5,25]. The targeted unit cell size was 5 × 5 × 5 mm, and given the abovementioned cell array this resulted in cubical specimens of 25 × 25 × 25 mm. The rhombic dodecahedron has a deviating cell length in one direction, which resulted in cubes measuring 25 × 17 × 17 mm (RD-X) and 17 × 25 × 17 mm (RD-YZ). The designed relative density of the structures varied between 2% and 20%, by changing the diameter of the circular struts constituting the porous structures. The final designs were exported as .STL files. All designs were additively manufactured at 3D Systems (Leuven, Belgium) using a DMP 320 machine (currently known as DMP Flex 350) and CP-Ti powder whose chemical composition complied with ASTM F67, ASTM B265, ASTM B348, ISO 5832-2, and ISO 13782 standards (Fig. 2A). This material type was chosen for its ductility and the ability to continuously deform without mechanical failure [23,26]. Moreover, CP-Ti has some other advantages over the more commonly used Ti-6Al-4V alloy, including the absence of hazardous alloying elements [23,27]. After printing, the parts were removed from the build plate using wire electrical discharge machining (EDM). In total, four specimens were printed for each design group, resulting in 140 specimens.

2.1.2. Deformable meta-implants

Three of the unit cell types were chosen for the design of deformable meta-implants based on their relatively high Poisson's ratios and low elastic moduli. They included the diamond, the body-centered cubic, and the rhombic dodecahedron (Fig. 2B-C). To enhance the deformability of the porous outer layer, a functionally graded structure was proposed. A unit cell size of 3 × 3 × 3 mm was used to ensure a gradually changing relative density in the 13.75 mm outer layer. The relative density was graded in three steps from 10% on the inside, to the minimum printable density at the bone-implant interface. The minimum printable relative density is determined by the minimum printable strut diameter, which is about 200 μm [28]. As a result, the minimum relative density slightly differs between the unit cell types (D/BCC = 2%, RD = 4%). The thickness of the three layers was made to decrease with the relative density to further increase the deformability at the bone-implant interface. This also mimics the hierarchical structure found in bone and matches its elasticity at the bone-implant interface [29,30]. For each of the unit cell types, two control cups were designed and were fully filled with either a 10% relative density structure (MAX) or with the minimum printable relative density (MIN). The exact dimensions can be found in Fig. 1D. For each of the designs, three specimens were printed, resulting in a total of 27 specimens.

2.1.3. Experimental setup

To assess the space-filing behavior of the proposed meta-implants, replicas of the common types of acetabular defects were made from a bone-mimicking material, namely cellular, rigid, polyurethane foam (20PCF, #1522-12, Sawbones Europe AB,

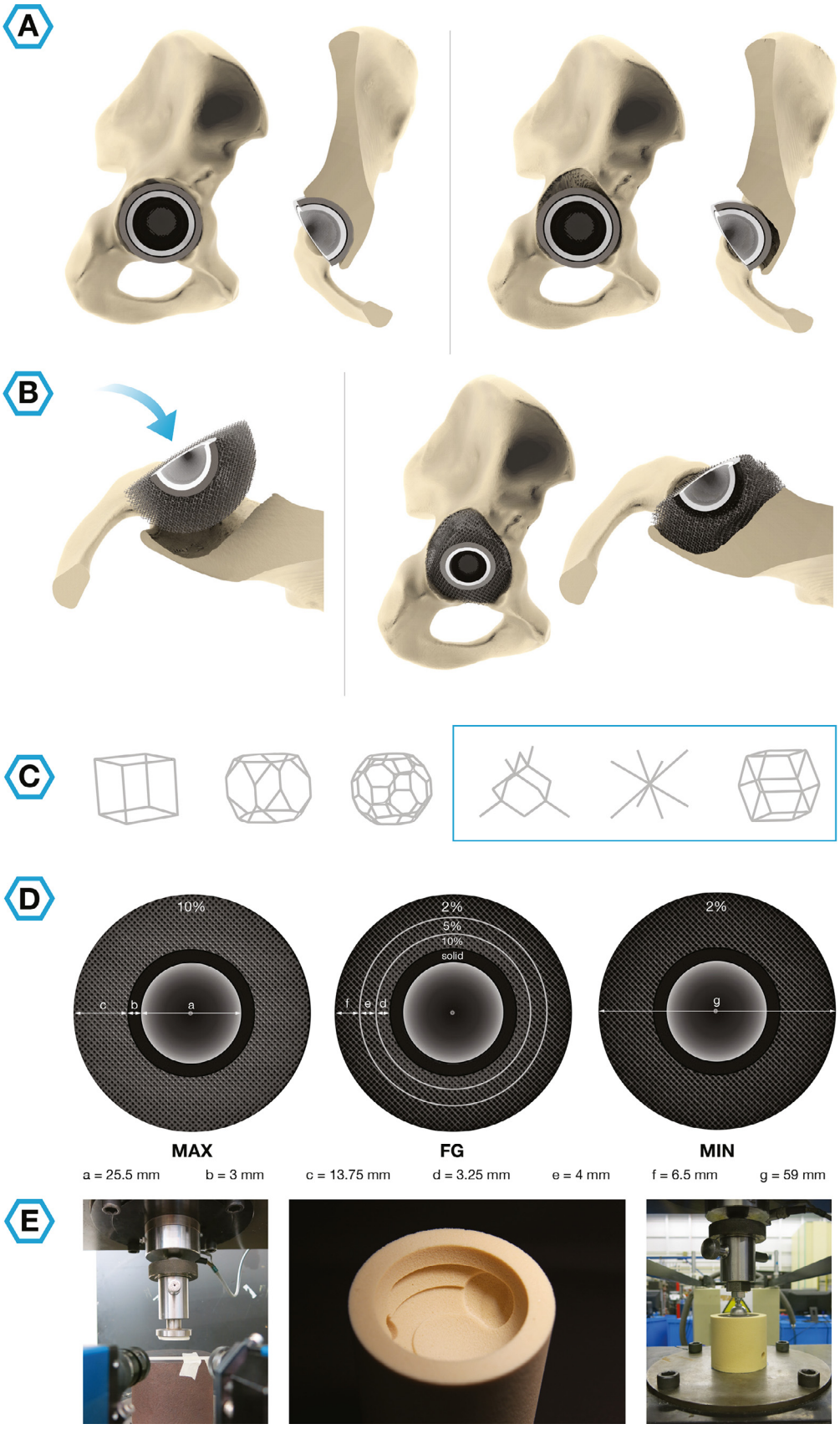

Fig. 1. A study outline showing the current implant designs (A) and the considerable defects that may grow over time. (B) The design proposed in this study can be deformed to fill up the defects and restore the physiological loading conditions. (C) Six non-auxetic unit cells (cube, truncated cube, truncated cuboctahedron, diamond, body-centered cubic, and rhombic dodecahedron) were evaluated in terms of their quasi-static mechanical properties to choose three unit cells for further assessment in the deformable meta-implants. (D) Each implant design comes in three different types of relative density (MAX, FG and MIN), which were eventually compressed in bone-mimicking molds to assess their deformability (E).

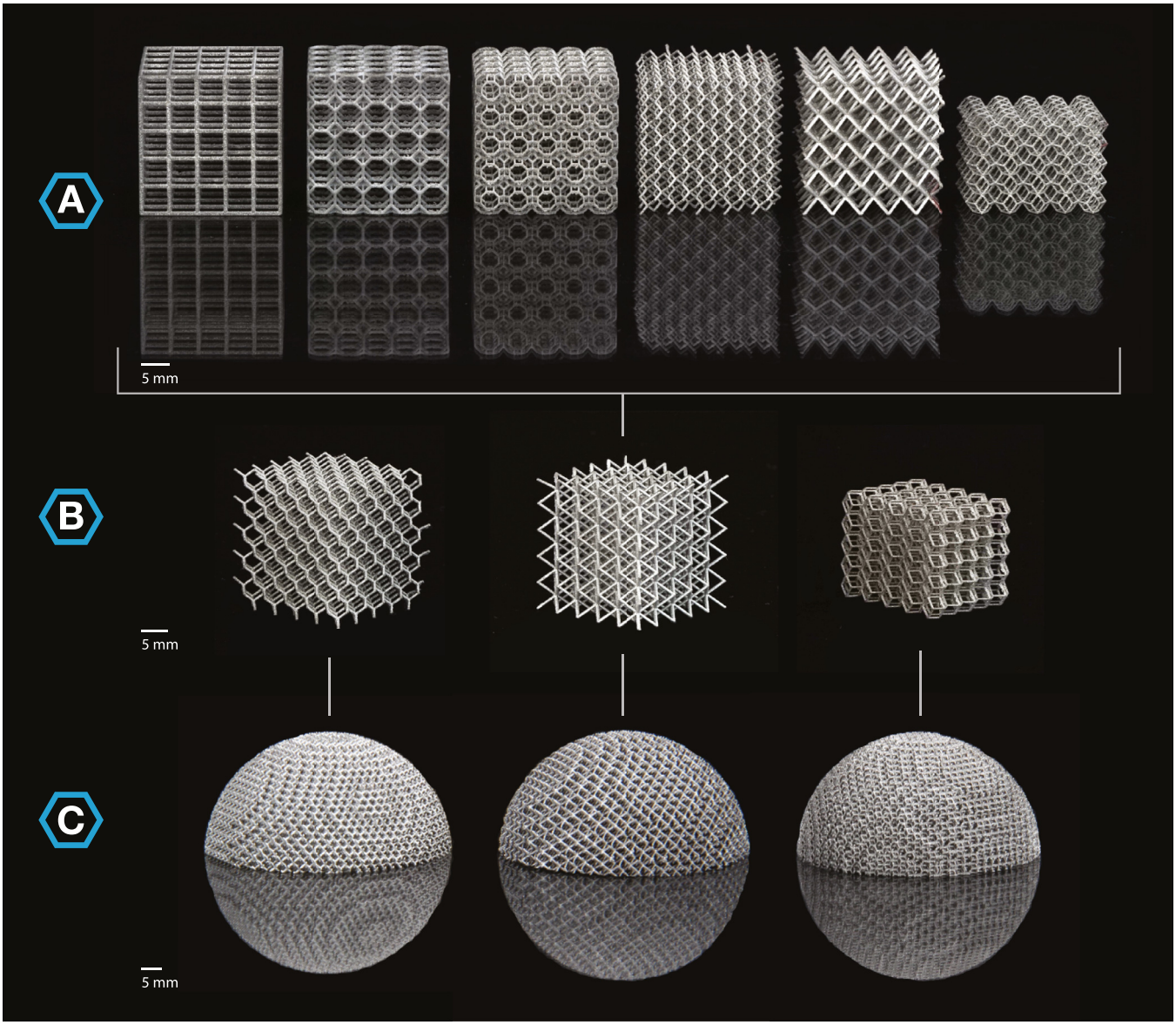

Fig. 2. An overview of the design choices as represented by the as-manufactured specimens. (A) The six different types of non-auxetic meta-biomaterials (rhombic dodecahedron visualized in the YZ orientation). (B) Three non-auxetic meta-biomaterials (diamond, body-centered cubic, and rhombic dodecahedron) were chosen to be incorporated in the deformable meta-implants (C-D).

Malmö, Sweden) (Fig. 1E). Sawbones delivered 27 solid cylinders (∅ 80mm, h = 80mm), in which a ∅ 60 mm semi-hemisphere was removed to mimic some of shape features of the acetabulum. Several holes and grooves were made using a milling machine, to simulate the Paprosky Type 2B defect found in the acetabulum after the removal of a primary implant [31]. The same procedure was repeated for all 27 molds. The defects were made to accommodate the deformation of the meta-implant throughout the entire range of the imposed displacements.

2.2. Morphological characterization

The relative density of the non-auxetic meta-biomaterials was determined by dry-weighing. The outer dimensions were measured using a caliper, while their weight was determined on a laboratory scale (Sartorius AG, Göttingen, Germany, accuracy = 0.1 mg). According to the dry-weighing technique, the relative density of a specimen can be calculated by dividing the weight of the specimen by the weight of a solid CP-Ti specimen with similar dimensions and a density of 4.51 g/cm^3 [32].

To study the morphology of the deformable meta-implants, two micro-CT scans were made using a Quantum FX micro CT scanner (Perkin Elmer, Waltham, United States), once before and once after compression into the mold. Subsequently, the micro-CT images could be used to assess the space-filling behavior of the meta-implants after compression. Tape was used to secure the cups inside the mold. The scans were performed with a voltage of 90 kV and a tube current of 200 μA. A 60 $\times$ 60 mm field of view (FOV) was used to visualize the overall deformation, using a voxel size of 120^3 μm^3. The sliced TIFF stacks were, then, imported into the image analysis software Fiji [33]. The histograms were equalized, a threshold was applied, and an additional Bernsen local thresholding was used to create binary images. A region of interest (ROI) was selected, in which the morphological characteristics were determined using the BoneJ plugin [34]. A 3D reconstruction of the images was created using the 3D viewer plugin to evaluate the location and degree of deformation of the meta-implants inside

the molds. In addition to this visual inspection, the deformation was quantitatively evaluated using the degree of anisotropy (DA) calculated with the BoneJ plugin. Additional scans were therefore made with a 40 × 40 mm FOV and a voxel size of 80^3 μm^3. The mean intercept length was used to estimate the degree to which substructures are preferentially oriented within a volume. The obtained values range between 0 and 1, from fully isotropic to fully anisotropic, respectively. The molds were eventually cut open to evaluate the extent to which they had been affected by the compression tests.

2.3. Mechanical testing

All non-auxetic meta-biomaterials were axially compressed using a mechanical testing machine (Zwick GmbH & Co. KG, Ulm, Germany) with a constant rate of 1 mm/min up until 40% strain. A 10, 20, or 250 kN load cell was used to match the load cell availability with the specifications of the experiments. The stress-strain curves were then used to acquire the quasi-static mechanical properties of the porous structures according to the ISO standard 13314:2011 [35]. The data were corrected for the machine compliance according to the 'direct technique' presented by Kalidindi et al. [36]. As a result, the maximum applied strain decreased. The "quasi-elastic gradient", from now on referred to as the elastic modulus, was calculated in the linear region between 20% and 70% of the first maximum compressive stress (FMCS). The ISO-13314:2011 standard also introduces the concept of "compressive offset stress", which was measured at 0.2% plastic compressive strain. This property will from now on be referred to as the yield strength.

The DIC technique was used to measure the full-field strains experienced during the compression of the non-auxetic meta-biomaterials [24]. DIC calculates the strain field by comparing the images of a specimen at different stages of deformation, while tracking an array of pixels. The specimens in this study do not have an intrinsic pixel pattern. Therefore, they had to undergo surface preparation: all specimens were painted black after which their front surface was stamped in white. A black, random, and unique pixel pattern was then added using an airbrush. Two 4 MP digital cameras (Limess, Krefeld, Germany) were used to capture the front surface of the specimens with a frequency of 1 Hz. The system was calibrated using the VicSnap software (Correlated Solutions Inc., Irmo, USA). The obtained images were analyzed using Vic-3D 8 (Correlated Solutions Inc., Irmo, USA) to calculate the values of directional strains (*i.e.,* ε_{xx} and ε_{yy}). For each of the lattice structures, a 3 × 3 cell array was selected as the region of interest, for which the strain values of the vertices were used to calculate the Poisson's ratio, ν (= $-\varepsilon_{xx}/\varepsilon_{yy}$). This was done for the images captured within the elastic region of the stress-strain curve using MATLAB 2017b (MathWorks, Natick, United States).

To test the deformability of the meta-implants, compression tests were performed on a static test machine (Zwick GmbH & Co. KG, Ulm, Germany) with a 20 kN load cell using the setup depicted in Fig. 1E. A 25 mm steel ball was used to apply a constant displacement of 0.5 mm/min to the inner hemisphere of the cup until a maximum displacement of 5 mm was achieved.

2.4. Statistical analyses

A two-way ANOVA was conducted to analyze the interaction between the effects of the relative density and unit cell type on each of the mechanical properties mentioned above. This statistical analysis was performed in SPSS 25.0 (IBM, Armonk, United States) and significance was assumed at $p < 0.05$. If a significant effect was found, an analysis of simple main effects was performed using a Sidak correction. The results have been presented according to the APA (American Psychological Association) standards, using the F-score (df, df error), as a measure of the ratio of variances, and the *p*-value.

3. Results

3.1. Non-auxetic meta-biomaterials

The as-manufactured relative density values, determined using the dry-weighing technique, varied between 20.0% and 2.4% (Table 1). The 20% CAD designs had a slightly lower relative density once manufactured, whereas almost all other designs gained some density during the printing process (Table 1). These deviations differed per unit cell type, although non-significantly. In all cases, the differences were < 5%.

The stress-strain curves of the non-auxetic meta-biomaterials (Fig. 3) and the derived mechanical properties (Fig.4A-B) were consistent between the specimens of each group. The cube and truncated cube exhibited a clear layer-by-layer collapse, whereas all specimens of the remaining four designs did not exhibit strut failure (Fig. 3). The diamond and rhombic dodecahedron (RD-YZ) exhibited a diagonal 'folding' line, while the body-centered cubic formed a flower-like shape around its center. A uniform deformation was observed in the rhombic dodecahedron (RD-X) specimens, showing a folding pattern in all of its layers. All data were normally distributed ($p > 0.05$). While the assumption of the homogeneity of the variances was violated ($p < 0.01$), the two-way ANOVA could still be performed due to the equal sample sizes and a variance ratio smaller than 3.

A statistically significant interaction was found between the effects of the unit cell type and relative density on the elastic modulus ($F(24,104) = 61.147$, $p < 0.001$) (Fig. 4A). Subsequently, the main effect for the unit cell type yielded an F-score of $F(6,104) = 890.102$, $p < 0.001$, indicating significant differences. The only unit cell types that did not exhibit significantly different elastic moduli were the diamond and the rhombic dodecahedron (both orientations). The differences were most apparent at a relative density of 20% ($F(6,104) = 381.284$, $p < 0.001$), and least apparent at a relative density of 2% ($F(6,104) = 5.610$, $p < 0.001$). The main effect of the relative density on the elastic moduli yielded an even bigger F-score of $F(4,104) = 1023.682$, $p < 0.001$, highly affecting the cube specimens ($F(4,104) = 626.978$, $p < 0.001$) and least affecting the body-centered cubic specimens ($F(4,104) = 15.881$, $p < 0.001$).

The type of the unit cell also significantly affected the yield strength ($F(6,104) = 329.814$, $p < 0.001$) (Fig. 4A). Non-significant differences were found between the diamond and both orientations of the rhombic dodecahedron. Again, the biggest differences were found at a relative density of 20% ($F(6,104) = 253.403$, $p < 0.001$), while values only slightly differed at a relative density of 2% ($F(6,104) = 0.913$, $p < 0.001$). The relative density yielded a significant main effect as well ($F(4,104) = 2193.557$, $p < 0.001$), especially in the truncated cube specimens ($F(4,104) = 646.540$, $p < 0.001$). The interaction effects of the unit cell type and relative density was also significant ($F(24,104) = 40.274$, $p < 0.001$).

The FMCS was significantly affected by the type of the unit cell ($F(6,104) = 308.446$, $p < 0.001$), the relative density ($F(6,104) = 2238.606$, $p < 0.001$), as well as their interaction ($F(24,104) = 46.493$, $p < 0.001$) (Fig. 4A). The differences in the FMCS between the diamond and the rhombic dodecahedron orientations were non-significant, as well as between the cube and truncated cube specimens. In general, the biggest differences were found at a relative density of 20% ($F(6,104) = 295.612$, $p < 0.001$) and the smallest at a relative density of 2% ($F(6,104) = 0.688$, $p < 0.001$). Significant differences, as a result of the relative density, were the

Table 1
The as-manufactured relative density of the non-auxetic meta-biomaterials.

	As-manufactured relative density [%]													
	C		TC		TCO		RD-YZ		RD-X		D		BCC	
CAD	mean	std.	mean	std.	mean	std.	mean	std.	mean	std.	mean	std.	mean	std.
20	20.00	0.10	19.99	0.18	19.61	0.11	18.50	0.21	19.21	0.18	16.75	0.10	16.19	0.27
15	15.37	0.07	15.38	0.05	15.86	0.03	14.66	0.11	15.20	0.08	12.95	0.03	12.83	0.07
10	10.97	0.09	10.91	0.10	10.86	0.03	10.06	0.10	10.62	0.11	8.79	0.03	9.18	0.07
5	5.96	0.07	6.06	0.01	6.14	0.08	5.84	0.04	6.15	0.06	5.12	0.08	5.19	0.03
2(4)	2.75	0.05	2.84	0.05	3.37	0.09	3.32	0.13	3.32	0.13	2.41	0.08	2.64	0.03

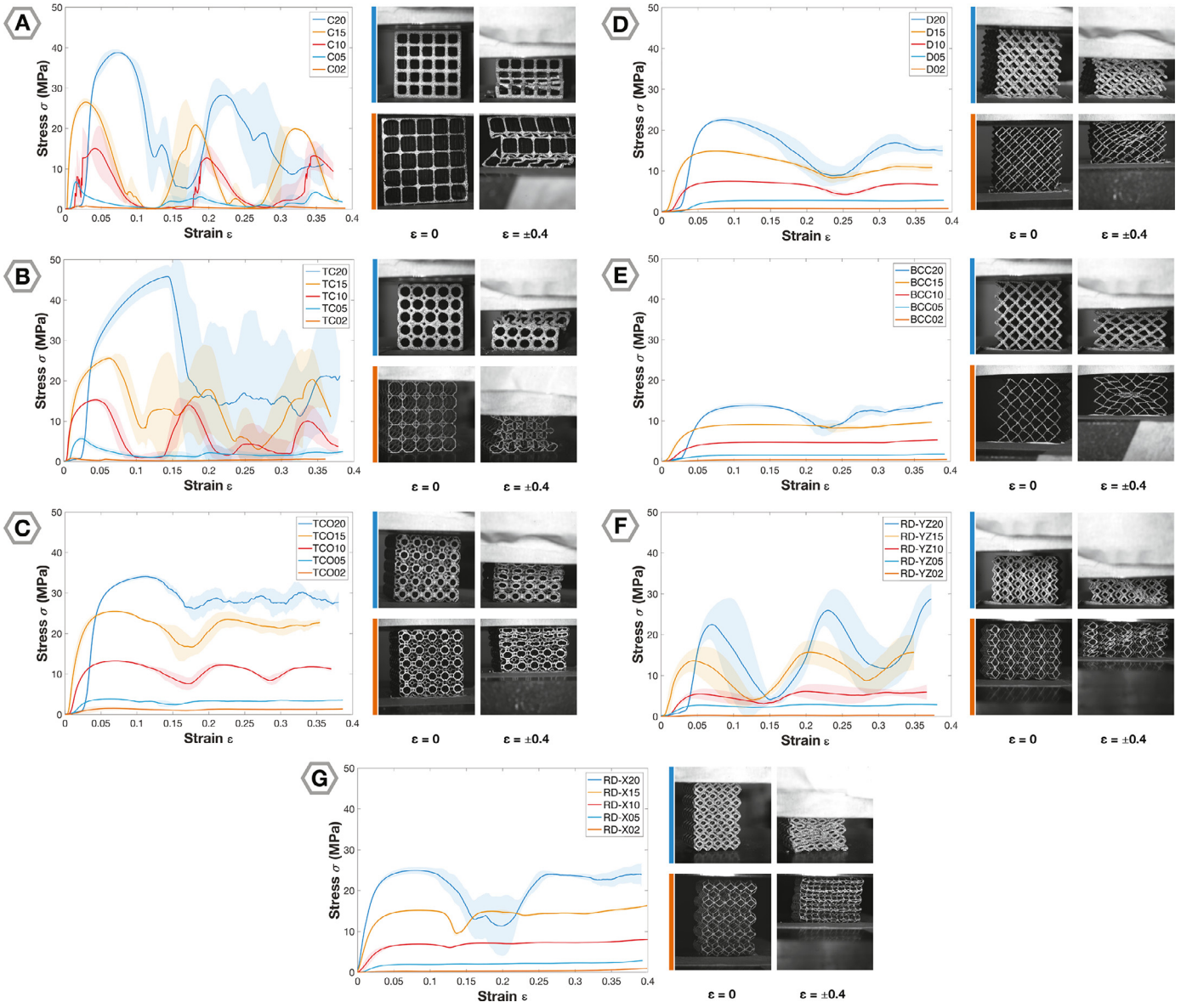

Fig. 3. The average stress-strain curves of the non-auxetic meta-biomaterials including the deformation of the designs with the relative densities of 2% and 20%. (A) cube, (B) truncated cube, (C) truncated cuboctahedron, (D) diamond, (E) body-centered cubic, (F) rhombic dodecahedron (RD-YZ), and (G) rhombic dodecahedron (RD-X).

greatest for the truncated cube specimens ($F(4,104) = 776.631$, $p < 0.001$).

The values of the Poisson's ratio (Fig. 4B) calculated using the DIC images (Fig. 4C-F) were significantly affected by the interaction of the effects of the unit cell type and relative density ($F(24,90) = 13.957$, $p < 0.001$). The unit cell type alone was also found to significantly affect the Poisson's ratio ($F(6,90) = 331.987$, $p < 0.001$), but non-significant differences were also found. The Poisson's ratio of the cube lattices was not found to be significantly different from the truncated cube lattices. The diamond lattices actually showed resemblance with the rhombic dodecahedron (RD-X) and the body-centered cubic lattices, in terms of their Poisson's ratio. The same held for the truncated cuboctahedron and the rhombic dodecahedron (RD-X). These similarities were the clearest at a relative density of 2% ($F(5,90) = 18.289$, $p < .001$), while the largest differences were found at a relative density of

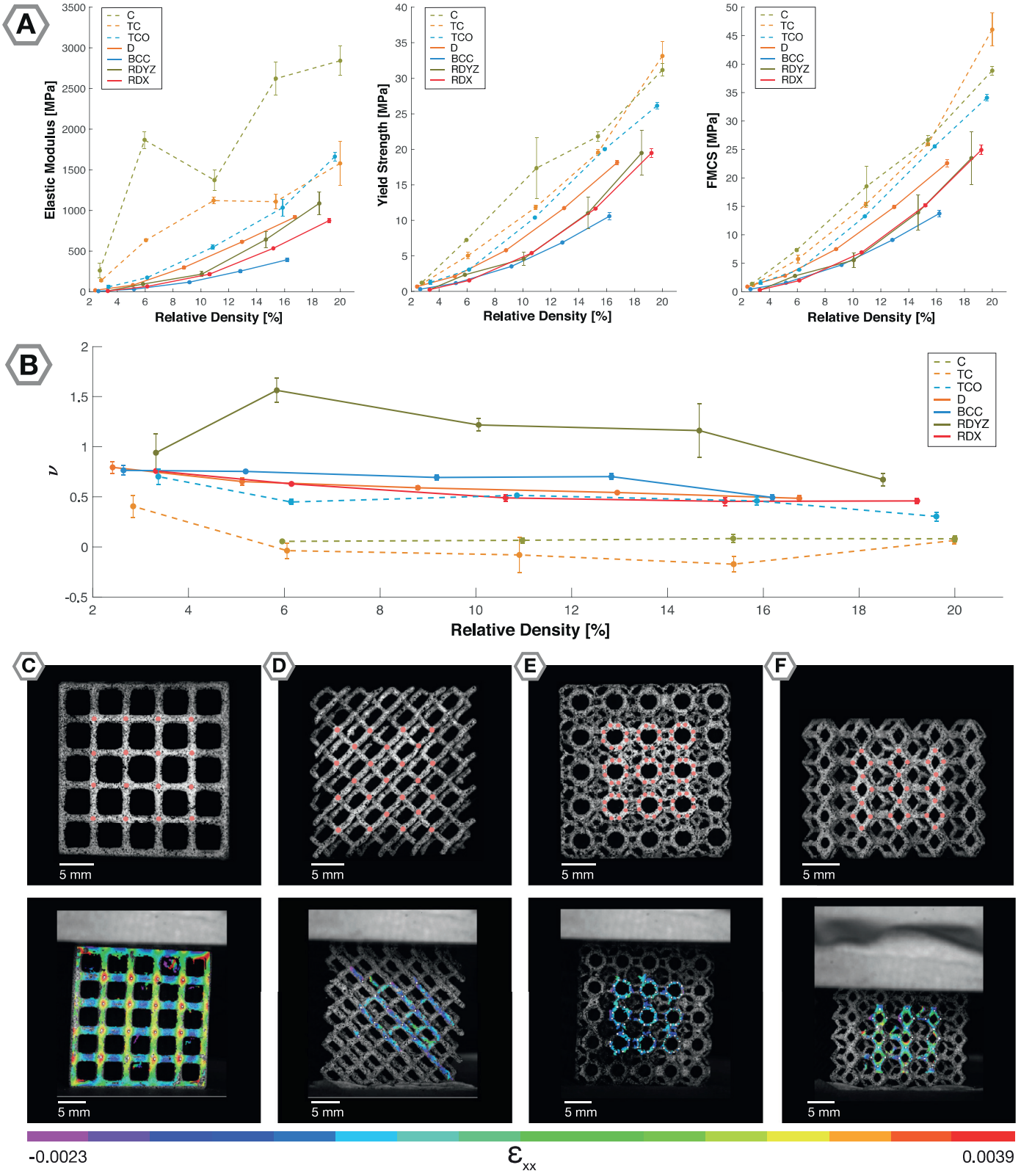

Fig. 4. The experimental mechanical properties of the non-auxetic meta-biomaterials as a function of their relative density ± SD. (A) The elastic modulus, yield strength, and first maximum compressive stress. (B) Poisson's ratio. (C-F) Some examples of the 3 × 3 cell arrays used to calculate the Poisson's ratio of the (LTR) cube, diamond, truncated cuboctahedron, and rhombic dodecahedron (RD-YZ) structures including the obtained horizontal strain values.

Table 2
The degree of anisotropy found in the acetabular implants before and after compression in the mold.

Type		Degree of Anisotropy				Difference [%]
		BEFORE	std.	AFTER	std.	
BCC	MAX	0.173	0.009	0.152	0.007	11.77
	MIN	0.184	0.054	0.137	0.007	19.66
	FG	0.161	0.011	0.100	0.007	19.24
D	MAX	0.153	0.009	0.159	0.003	-3.85
	MIN	0.138	0.054	0.064	0.028	52.30
	FG	0.118	0.011	0.080	0.023	32.93
RD	MAX	0.389	0.031	0.362	0.038	5.86
	MIN	0.537	0.036	0.506	0.008	4.59
	FG	0.493	0.048	0.383	0.038	22.14

5% ($F(6,90) = 146.838$, $p < .001$). The relative density itself also significantly affected the Poisson's ratio ($F(4,90) = 41.028$, $p < 0.001$), especially in the rhombic dodecahedron (RD-YZ) specimens ($F(4,90) = 64.205$, $p < 0.001$).

3.2. Deformable meta-implants

The highest push-in forces (14.3 kN) were measured during the compression of the cups with the highest relative density (MAX), while the lowest maximum forces (3.3 kN) were observed during the compression of the cups with the lowest relative density (MIN) (Fig. 5A). The functionally graded (FG) designs performed in between these two densities. For all three design types (MAX, MIN, FG), the lowest push-in forces were measured for the body-centered cubic cups, followed by the diamond and rhombic dodecahedron, respectively.

Based on the 2D and 3D representations of the deformations (Fig. 5B-D) and the measured values of DA (Table 2), the smallest deformations were found in the MAX designs. Cutting the molds revealed that most of the deformation took place in the mold itself, instead of the cup. The molds did not show any signs of failure. The biggest deformations were found in the MIN designs, but visual inspection showed that the unit cells surrounding the solid hemisphere started bulging upwards during the compression tests (Fig. 5B-D). The micro-CT images showed that the deformations had mainly occurred in the struts connected to the solid hemisphere. After the mold was cut open, one could see that the porous outer layer had not been fully deformed into the defects. The rhombic dodecahedron cups were an exception, in which the DA values showed relatively small deformations in the MIN design. The FG designs were found to show the biggest deformation at the mold-implant interface, filling the defects, without any visual collapse surrounding the solid hemisphere.

4. Discussion

4.1. Geometry-property relationships

The as-manufactured relative density of the non-auxetic meta-biomaterials determined using the dry-weighing technique were generally higher than their designed values (with some exceptions). The observed difference decreased with the relative density. These deviations may have been caused by geometrical imperfections (*e.g.*, powder adhesion, strut thickness heterogeneity, and over-melting) inherent to all metal powder bed fusion processes [28,37–41]. This explanation is especially consistent with the assumption that the size of these imperfections is more or less constant across the entire strut thickness spectrum [42], resulting in a stronger effect in the designs with smaller struts diameters and, thus, lower relative densities. Moreover, the differences between the designed and as-manufactured values of the relative density differed depending on the type of the unit cell. The diamond lattices showed the biggest deviations from their CAD file (mean absolute difference = 1.4%), while the cube lattices were almost a one-to-one match (mean absolute difference = 0.6%). The oblique struts, which are dominant in unit cells like the diamond, are generally built by the stacking of melt pools across multiple layers [28,38]. Additionally, printing of these struts forces the laser to make frequent acute turns, thereby enlarging the melt pool [28,37,38]. In the end, both events contribute to an increase in strut thickness. Oblique struts are usually of lower quality as well, compared to vertically oriented struts, which could influence the below-mentioned mechanical properties [43].

The mechanical properties of the non-auxetic meta-biomaterials were determined according to terms and descriptions presented in the ISO-13314:2011 standard [35]. A typical stress-strain curve of porous structures starts with a linear region, which is followed by fluctuations in the plateau region and finally ends in a sharp increase towards densification [44]. The obtained stress-strain curves showed similar, but also different behaviors. The deformation mechanism of lattices is usually a combination of bending and stretching [45,46]. The dominant deformation mechanism depends on the connectivity of the unit cells as well as the orientation of the struts with respect to the loading direction [45,46]. With the main strut orientation aligned along the loading direction, structures like the cube and truncated cube are more stretch-dominated. Their stress-strain curve shows a sharp increase in stress up until very high loads, followed by a layer-by-layer collapse, typical for brittle structures [47]. Lattices like the diamond, body-centered cubic, and rhombic dodecahedron (both orientations) exhibit an inclined main strut orientation and thus, mainly deform through bending. Their stress-strain curve shows a gradual increase in stress followed by a plateau. The truncated cuboctahedron was found to perform in between those two categories, showing a behavior similar to those of the stretch-dominated structures for the higher values of the relative density while resembling the behavior of the bending-dominated structures for the lower values of the relative density. For the lower values of the relative density, the rhombic dodecahedron (RD-YZ) structures showed fluctuations without a clear plateau. The final densification phase cannot

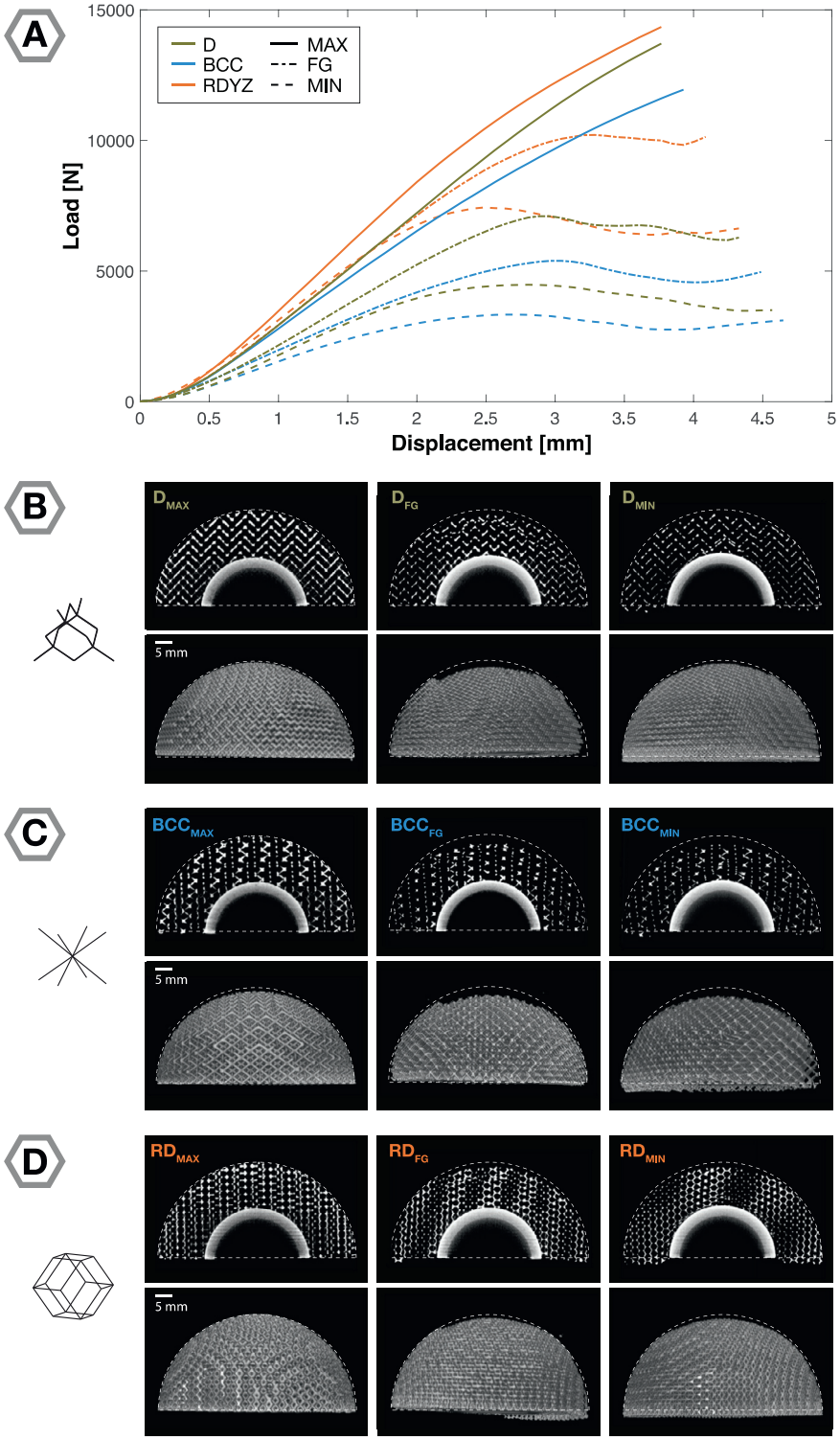

Fig. 5. The deformation data measured for the deformable meta-implants. (A) Load displacement curves, (B-D) micro-CT images, and the 3D reconstructions of the diamond, body-centered cubic, and rhombic dodecahedron cups before and after deformations.

be seen in these stress-strain curves, but are expected to appear for some higher values of the applied strain [44].

According to the Gibson and Ashby model [48], the elastic modulus, yield strength, and FMCS all increase with the relative density. Deviations from this trend were found in the cube and truncated cube lattices. Whereas all other groups were tested with a 250 kN load cell (high relative density specimens) or 10/20 kN load cells (low relative density specimens), the load cell selection was less consistent for those designs due to machine availability. Together with the machine compliance correction applied afterwards, this might have led to a non-continuous trend line.

Based on the quasi-static properties, and the accompanying stress-strain curves, two groups could be distinguished. The first group consists of the lattice structures with high values of the elastic modulus, including the cube, truncated cube, and truncated cuboctahedron unit cells. The latter approaches the second group

for the lower values of the relative density. The second group includes the diamond, body-centered cubic, and rhombic dodecahedron (both orientations) unit cells, exhibiting lower values of the elastic modulus. In general, the cubic lattices exhibited the highest elastic moduli, while the body-centered cubic lattices were found to have the lowest stiffness. The obtained values followed the same order as reported in the literature [3,49]. The rhombic dodecahedron lattices are, however, an exception. Whereas other studies show that the rhombic dodecahedron unit cell performs in between the truncated cube and diamond unit cells, the lattices in our study only outperform the body-centered cubic lattices [3,49]. The rhombic dodecahedron (RD-YZ) lattices did exhibit a higher stiffness than their counterparts in the X orientation, which is in line with the literature [3,49–51]. As compared to their Ti-6Al-4V counterparts, the lattices in this study exhibited slightly lower elastic moduli and strength [3]. This is expected given the difference in the bulk properties of Ti-6Al-4V and CP-Ti [32,52].

All unit cell types showed decreasing values of the Poisson's ratio with the relative density, which is expected given the theoretical predictions of such structures [3,49]. The truncated cube lattices exhibited an auxetic behavior for the relative densities between 5% and 15%, which is unexpected given that this unit cell is generally considered to be non-auxetic [3,53]. The rhombic dodecahedron (RD-YZ) lattices exhibited Poisson's ratios as high as 1.56, reflecting their anisotropy while showing an abrupt drop at a relative density of 2%. This probably relates to the decreased reliability of the DIC method for the very low values of the relative density where, due to the small strut thickness, the number of traceable pixels is limited. Additionally, these specimens quickly reach their yield point. Since the Poisson's ratio is calculated in the elastic region, the number of the data points available for calculating the Poisson's ratio is limited. Consequently, the values of the Poisson's ratio measured for such highly porous structures tend to be less accurate and may deviate from theoretical predictions [3,49]. The rhombic dodecahedron (RD-X) lattices on the other hand, exhibited values between 0.46 and 0.76. The significant difference between these two rhombic dodecahedron orientations has been reported in the literature [3,50,51], but the absolute values differ. Babaee et al. reported values of ± 0.5 for RD-X and ± 1.0 for RD-YZ [50], while other computational and numerical data pointed at values ranging between 0.00 and 0.40 for RD-X and between 0.42 and 1.0 for RD-YZ [3,49,51]. Given that the Poisson's ratio of porous structures is a function of their relative density, the exact values of the Poisson's ratio reported in different studies are also dependent on the range of the relative densities considered within each study. The values of the Poisson's ratios obtained in this study, while not exactly matching the data in the literature, are in line with the findings of previous studies [3,50,51]. They also follow the same main trend in which bending-dominated unit cells exhibit a greater lateral expansion in response to axial compression than the stretch-dominated designs [3,49]. The values measured here do seem to be overestimating the Poisson's effect, which can be explained by the use of DIC. This technique generally overestimates small-magnitude homogeneous strain-fields by about 3-4% [54]. Overall, the highest Poisson's ratio values were found for the rhombic dodecahedron (RD-YZ) lattices followed by the body-centered cubic, diamond, rhombic dodecahedron (RD-X), and truncated cuboctahedron lattices, respectively. The truncated cube lattices exhibited the smallest space-filling potential, due to their extraordinary auxetic response.

Based on all of the aforementioned properties (*i.e.*, a low elastic modulus and high values of the Poisson's ratio), the diamond, body-centered cubic, and rhombic dodecahedron unit cells were chosen to be implemented in the deformable meta-implants. The relatively high values of their Poisson's ratios suggest that these unit cells have the ability to increase their volume in directions perpendicular to the load. Together with their high strength, low stiffness, and the ability to deform without failure, they were expected to perform the best in the design of space-filling, deformable meta-implants.

4.2. Space-filling behavior

The load-displacement curves showed a clear distinction between the designs, with the lowest push-in forces measured in the designs based on the body-centered cubic unit cell, while the highest push-in forces were recorded for the rhombic dodecahedron group. The deformable meta-implants, therefore, do not follow the same order as found in the first part of this study regarding the non-auxetic meta-biomaterials. Despite their similar mechanical properties, the diamond and rhombic dodecahedron unit cells exhibited a substantial difference in their push-in force, especially in the FG and MIN designs. The slightly higher minimum relative density in the rhombic dodecahedron designs (4%) may be the reason for this. Additionally, the rhombic dodecahedron unit cell is highly anisotropic and may, therefore, behave very differently in this hemispherical configuration. This does, however, reflect the mechanical properties of the rhombic dodecahedron found in the literature, which are generally higher than those found for the diamond unit cell [3,49]. Regarding the three relative density profiles (*i.e.*, MAX, FG, MIN), the lowest push-in forces were found for the designs with the smallest strut thickness, and, thus, the lowest relative density (MIN). Due to the small thickness to length ratios, the struts in these designs have a lower bending stiffness. Together with the tendency to buckle as a result of the increased slenderness ratio, these structures will more easily deform. The ease of deformation will, therefore, decrease with the relative density.

Due to the absence of comparable literature, a new approach had to be found to quantify the meta-implant's deformation. The DA was determined before and after the deformation and showed that the substructures were more isotropic after compression into the mold. This can be explained by the fact that the struts start to align during compression, whereas the initial design includes various strut orientations. In general, the biggest change in the preferential orientation was found in the MIN designs. However, differences with the other two relative density types were not always significant and a deviation from this trend was found for the rhombic dodecahedron unit cell. The reliability of this method should, therefore, be evaluated. Nevertheless, the values show that the biggest deformation took place in the cups designed using the diamond unit cell, followed by the body-centered cubic and finally the rhombic dodecahedron unit cell.

The micro-CT images indicated where the deformation exactly took place. The deformation of the MIN designs primarily took place in the struts directly connected to the solid hemisphere. Due to this failure, the solid hemisphere was compressed through the porous outer layer and a bulging effect occurred at the bottom. Due to the low relative density, the outer layer was simply not strong enough to transfer the forces from the solid hemisphere to the mold-implant interface. The MAX designs, on the other hand, were too stiff to deform in the relatively 'soft' mold. Their visual deformation supported the low DA values that were measured. The FG designs seem to provide the desired deformation pattern. The struts surrounding the solid hemisphere remained intact, while the unit cells directly in contact with the mold deformed into the defects. Despite being detectable, this deformation was limited. This was, however, expected given the relatively small compression that was applied. Due to the small differences in the Poisson's ratios, we could not observe a significant correlation between this property and the space-filling behavior of the meta-implants. However, according to both visual and quantifiable data, the diamond-FG cup

exhibited the most promising deformability and space-filling properties.

4.3. Challenges and limitations

Due to the explorative nature of this study, it was quite challenging to find suitable and reliable methods to assess the performance of the specimens. DIC has been used before to determine the strain distributions of lattices [55–57], but only a few studies actually calculated the Poisson's ratio [7,58,59]. Furthermore, it never involved structures with very low values of the relative density. Some of the non-auxetic meta-biomaterials in this study have very thin struts and, thus, a limited number of traceable pixels. Together with the relatively small elastic region, this resulted in large intra-specimen variability. For the cubic lattices with a relative density of 2%, it was even impossible to retrieve a sufficient number of data points to calculate the Poisson's ratio. By increasing the strut thickness, and, thus, the surface of traceable pixels, the reliability of the results improved with smaller intra-specimen differences.

Furthermore, the non-auxetic meta-biomaterials were compressed in the build direction. This may not be a problem considering the isotropic nature of most of the unit cell types, but the printing process itself has also been found to introduce a certain level of anisotropy [5,43]. The inferior print quality of horizontally built struts will affect the overall quality of the constructs, and, thus, their direction-dependent mechanical properties [38,43,60]. The non-auxetic meta-biomaterials should, therefore, be tested in multiple directions to obtain a clear overview of their behavior.

This study can be regarded as the first attempt to additively manufacture and experimentally assess a deformable (FG) space-filling meta-implant. First, decisions had to be made to effectively assess the deformability of the implants while mimicking the correct anatomical situation. A bone-mimicking foam was chosen over cadaveric bone for testing the performance of the developed meta-implants, because it offers a higher level of reproducibility and a lower degree of inter-specimen variability (both geometrical and in terms of the mechanical properties). With a Young's modulus of 0.137 GPa, the elastic modulus of the bone-mimicking material falls in the range of the values reported for the healthy trabecular bone [61]. However, the patients in need of a hip replacement often have significant acetabular bone deficiencies and poor (osteoporotic) bone quality. The use of this material may, therefore, not exactly represent the mechanical properties of (all) patients. Patel et al. argued that bone-mimicking foams with a lower density (10PCF) may better represent the bone properties of this group of patients [62]. In general, it is possible to design different classes of such implants with different mechanical properties of the porous outer layer. The appropriate class of deformable implants can be chosen based on the quality of the patient's bones.

Another limitation involves the high push-in forces that were needed to compress and deform the meta-implants into the mold. For a surgeon, it will be difficult, if not impossible, to apply such forces using a constant deformation rate. Currently, acetabular cups are implanted using impact forces with a mean magnitude of 16.8 kN. A successful implantation may take up to five impacts with peak forces reaching 27.5 kN [63]. However, such a procedure may lead to unpredictable deformations in the case of deformable implants. Additionally, peak forces may cause strut failure, which could induce an inflammatory reaction at the bone-implant interface [64]. Even though the force magnitudes are not directly comparable due to their different nature (i.e. impact forces vs. quasi-statically applied), this comparison does serve the intention of showing the relatively high forces required for the deformation of our implants.

One could think of two possible scenarios to ensure implant stability and integrity: a new surgical procedure or an optimized implant designed for increased deformability (or a combination thereof). Screw fixtures along the rim of the implant could be used to apply a more uniform deformation, but the removal of the screws after the implantation will be crucial to prevent stress shielding. The optimization of the implant design can be achieved by increasing the unit cell size to decrease the overall bending stiffness or by decreasing the strut thickness, provided that the printing tolerances improve. It should, however, be noted that the thickness of the porous layer does not change. As a result, the number of stacked unit cell layers decreases, and the relative density may need to be changed within the same unit cell.

4.4. Potential applications and future research

The mechanical properties that have been obtained in this study for a number of non-auxetic meta-biomaterials add to the growing library of geometry-property relationships available for lattice structures. With this library, we can facilitate the selection of non-auxetic meta-biomaterials for specific implant applications.

The use of a more ductile material, such as CP-Ti, contributes to the overall deformability of the meta-implants proposed here. Although the space-filling behavior of the implants is not yet optimal, there are some clear paths towards design optimization potentially with the help of computational models to achieve the space-filling behavior that is required for the intended orthopedic applications. Besides strut-based unit cells, one could also think of using sheet-based constructs. The curvature of triply periodic minimal surfaces (TPMS) is believed to mimic the trabecular morphology, and is, therefore, a promising alternative [65]. These curved surfaces result in enhanced tissue regeneration. Given their positive Poisson's ratios [66], TPMS may also exhibit promising space-filling properties [4].

The use of a functionally graded relative density improved the performance of the space-filling deformable meta-implants while simultaneously mimicking the hierarchical structure of bone [29]. A previous study by Wang et al. showed that the use of a functionally graded relative density could provide many advantages over existing acetabular cup designs [30]. The other two designs (MAX, MIN) showed the undesirable effects of using a single relative density and helped in putting the added value of a functionally graded design in perspective. After optimization, the FG cup may be used to treat acetabular defects with large bone deficiencies. The areas of application include not only the Paprosky type 2 defects but also cases in which the medial wall is no longer intact [31]. The induced plastic deformation makes sure that the implant settles in the bone defect, enhancing the force distribution at the bone-implant interface. Mimicking the physiological loading situation is important for stimulating bony ingrowth and is, therefore, expected to contribute to the secondary fixation of the meta-implant. A dual mobility cup could then be cemented in place, similar to the custom-made triflange implants [17]. When done properly, this concept could become the next standard in the treatment of both primary and secondary hip replacements.

Before the idea of space-filling deformable meta-implants can be put into practice, one has to assess the mechanical and biological properties of such implants over time. During their lifetime, acetabular implants are subjected to millions of loading cycles [67]. The fatigue performance of such implants is, therefore, an important aspect that needs to be carefully evaluated. For some of the non-auxetic meta-biomaterials the fatigue performance has already been studied [5,23,68–71]. Those studies have shown the importance of material type, printing imperfections, and geometrical design in determining the fatigue behavior of porous biomaterials [72]. CP-Ti has been proposed as the material of choice in cycli-

cally loaded applications [23], as its plasticity decreases the crack initiation and propagation. However, future research should assess the fatigue performance of the porous structures used in the design of a space-filling meta-implant.

The effects of the pore size are also worth mentioning. The deformation of the porous outer layer will decrease the pore size within the porous structure and may potentially lead to the closure of some pores. This could have substantial biological consequences [73]. Other time-dependent phenomena, such as tissue ingrowth, should, therefore, be evaluated before pursuing the proposed concept further.

Based on the obtained properties of the non-auxetic meta-biomaterials considered here, one could think of many possible applications. Load-bearing locations like the acetabulum are an example, but any type of bone defect could benefit from the deformability of CP-Ti lattices. In the locations where the mechanical performance is solely based on the quasi-static properties of the biomaterial, one could instantly benefit from the meta-biomaterials designed here. With the additional 'plastic' benefits when manufactured in CP-Ti, these non-auxetic meta-biomaterials could potentially serve other industries too.

5. Conclusions

We assessed the mechanical properties of additively manufactured architected materials made from six different non-auxetic unit cells and evaluated their performance in the design of a deformable meta-implant. With the aim of restoring the physiological loading conditions in critically sized acetabular defects, the meta-implants were given a highly porous outer layer with enhanced space-filling properties. The diamond, body-centered cubic, and rhombic dodecahedron lattices were found to exhibit the most ideal combination of properties including a low stiffness and a high positive Poisson's ratio. They were, therefore, implemented in the design of deformable meta-implants with three types of density distributions. The meta-implants were compressed in a bone-mimicking mold mimicking the Paprosky Type 2B defects. Micro-CT images revealed that the most promising deformation pattern was found in the functionally graded meta-implants based on the diamond unit cell. Despite a satisfactory deformation at the mold-implant-interface, the push-in forces were too high (3.3–14.3 kN). Design optimization should, therefore, be an important part of future research to optimize the space-filling behavior of the meta-implants and to facilitate the implantation process for orthopedic surgeons. Taking this into consideration, this deformable implant design has the potential to improve the biological fixation and decrease stress shielding in the acetabular component of a THR.

Disclosures

None.

Declaration of Competing Interest

The authors declare the following financial interests/personal relationships which may be considered as potential competing interests: Harrie Weinans is co-inventor on a patent co-owned by the UMC Utrecht that protects the use of a deformable acetabular implant (BE 2020/5810) and may receive income via a license agreement of UMC Utrecht with a commercial party.

Acknowledgements

The research for this paper was financially supported by the Prosperos project, funded by the Interreg VA Flanders – The Netherlands program, CCI grant no. 2014TC16RFCB04.

References

[1] A.A. Zadpoor, Mechanical meta-materials, Mater. Horizons 3 (5) (2016) 371–381.
[2] H.M. Kolken, A. Zadpoor, Auxetic mechanical metamaterials, RSC Adv. 7 (9) (2017) 5111–5129.
[3] C.P. de Jonge, H. Kolken, A.A. Zadpoor, Non-auxetic mechanical metamaterials, Materials 12 (4) (2019) 635.
[4] F. Bobbert, K. Lietaert, A.A. Eftekhari, B. Pouran, S. Ahmadi, H. Weinans, A. Zadpoor, Additively manufactured metallic porous biomaterials based on minimal surfaces: a unique combination of topological, mechanical, and mass transport properties, Acta Biomater. 53 (2017) 572–584.
[5] S.A. Yavari, S. Ahmadi, R. Wauthle, B. Pouran, J. Schrooten, H. Weinans, A. Zadpoor, Relationship between unit cell type and porosity and the fatigue behavior of selective laser melted meta-biomaterials, J. Mech. Behav. Biomed. Mater. 43 (2015) 91–100.
[6] A.A. Zadpoor, Design for additive bio-manufacturing: From patient-specific medical devices to rationally designed meta-biomaterials, Int. J. Mol. Sci. 18 (8) (2017) 1607.
[7] H.M. Kolken, S. Janbaz, S.M. Leeflang, K. Lietaert, H.H. Weinans, A.A. Zadpoor, Rationally designed meta-implants: a combination of auxetic and conventional meta-biomaterials, Mater. Horizons 5 (1) (2018) 28–35.
[8] G.K. Deirmengian, B. Zmistowski, J.T. O'Neil, W.J. Hozack, Management of acetabular bone loss in revision total hip arthroplasty, JBJS 93 (19) (2011) 1842–1852.
[9] W.G. Paprosky, S.H. Weeden, J.W. Bowling Jr, Component removal in revision total hip arthroplasty, Clin. Orthopaed. Related Res. 393 (2001) 181–193 (1976-2007).
[10] K.J. Bozic, S.M. Kurtz, E. Lau, K. Ong, T.P. Vail, D.J. Berry, The epidemiology of revision total hip arthroplasty in the United States, JBJS 91 (1) (2009) 128–133.
[11] L. Pulido, S.R. Rachala, M.E. Cabanela, Cementless acetabular revision: past, present, and future, Int. Orthop. 35 (2) (2011) 289–298.
[12] A. Volpin, S. Konan, C. Biz, R. Tansey, F. Haddad, Reconstruction of failed acetabular component in the presence of severe acetabular bone loss: a systematic review, Musculoskeletal Surg. 103 (1) (2019) 1–13.
[13] M. Baauw, M.L. van Hooff, M. Spruit, Current construct options for revision of large acetabular defects: a systematic review, JBJS Rev. 4 (11) (2016).
[14] N.P. Sheth, C.L. Nelson, B.D. Springer, T.K. Fehring, W.G. Paprosky, Acetabular bone loss in revision total hip arthroplasty: evaluation and management, JAAOS-J. Am. Acad. Orthopaed. Surg. 21 (3) (2013) 128–139.
[15] Y. Kosashvili, D. Backstein, O. Safir, D. Lakstein, A. Gross, Acetabular revision using an anti-protrusion (ilio-ischial) cage and trabecular metal acetabular component for severe acetabular bone loss associated with pelvic discontinuity, J. Bone Joint Surgery. Br. 91 (7) (2009) 870–876.
[16] X. Flecher, S. Sporer, W. Paprosky, Management of severe bone loss in acetabular revision using a trabecular metal shell, J. Arthroplasty 23 (7) (2008) 949–955.
[17] M. Baauw, G.G. van Hellemondt, M. Spruit, A custom-made acetabular implant for Paprosky type 3 defects, Orthopedics 40 (1) (2017) e195–e198.
[18] J. Wolff, in: Das Gesetz Der Transformation Der Knochen, 1, A Hirshwald, 1892, pp. 1–152.
[19] R. Huiskes, H. Weinans, B. Van Rietbergen, The relationship between stress shielding and bone resorption around total hip stems and the effects of flexible materials, Clin. Orthop. Relat. Res. (1992) 124–134.
[20] D. Sumner, Long-term implant fixation and stress-shielding in total hip replacement, J. Biomech. 48 (5) (2015) 797–800.
[21] R. Huiskes, R. Ruimerman, G.H. Van Lenthe, J.D. Janssen, Effects of mechanical forces on maintenance and adaptation of form in trabecular bone, Nature 405 (6787) (2000) 704–706.
[22] A.A. Zadpoor, Bone tissue regeneration: the role of scaffold geometry, Biomater. Sci. 3 (2) (2015) 231–245.
[23] R. Wauthle, S.M. Ahmadi, S.A. Yavari, M. Mulier, A.A. Zadpoor, H. Weinans, J. Van Humbeeck, J.-P. Kruth, J. Schrooten, Revival of pure titanium for dynamically loaded porous implants using additive manufacturing, Mater. Sci. Eng.: C 54 (2015) 94–100.
[24] N. McCormick, J. Lord, Digital image correlation, Mater. Today 13 (12) (2010) 52–54.
[25] S. Ahmadi, S. Yavari, R. Wauthle, B. Pouran, J. Schrooten, H. Weinans, A. Zadpoor, Additively manufactured open-cell porous biomaterials made from six different space-filling unit cells: the mechanical and morphological properties, Materials 8 (4) (2015) 1871–1896.
[26] H. Attar, L. Löber, A. Funk, M. Calin, L. Zhang, K. Prashanth, S. Scudino, Y. Zhang, J. Eckert, Mechanical behavior of porous commercially pure Ti and Ti–TiB composite materials manufactured by selective laser melting, Mater. Sci. Eng.: A 625 (2015) 350–356.
[27] F. Li, J. Li, T. Huang, H. Kou, L. Zhou, Compression fatigue behavior and failure mechanism of porous titanium for biomedical applications, J. Mech. Behav. Biomed. Mater. 65 (2017) 814–823.
[28] S. Van Bael, G. Kerckhofs, M. Moesen, G. Pyka, J. Schrooten, J.-P. Kruth, Micro-CT-based improvement of geometrical and mechanical controllability of selective laser melted Ti6Al4V porous structures, Mater. Sci. Eng.: A 528 (24) (2011) 7423–7431.
[29] J.-Y. Rho, L. Kuhn-Spearing, P. Zioupos, Mechanical properties and the hierarchical structure of bone, Med. Eng. Phys. 20 (2) (1998) 92–102.

[30] H.V. Wang, S.R. Johnston, D.W. Rosen, Design of a graded cellular structure for an acetabular hip replacement component, in: 17th Solid Freeform Fabrication Symposium, 2006, pp. 111–123.
[31] W.G. Paprosky, P.G. Perona, J.M. Lawrence, Acetabular defect classification and surgical reconstruction in revision arthroplasty: a 6-year follow-up evaluation, J. Arthroplasty 9 (1) (1994) 33–44.
[32] 3DSystems, LaserForm Ti Gr1 (A), 2017.
[33] J. Schindelin, I. Arganda-Carreras, E. Frise, V. Kaynig, M. Longair, T. Pietzsch, S. Preibisch, C. Rueden, S. Saalfeld, B. Schmid, Fiji: an open-source platform for biological-image analysis, Nat. Methods 9 (7) (2012) 676–682.
[34] M. Doube, M.M. Kłosowski, I. Arganda-Carreras, F.P. Cordelières, R.P. Dougherty, J.S. Jackson, B. Schmid, J.R. Hutchinson, S.J. Shefelbine, BoneJ: free and extensible bone image analysis in ImageJ, Bone 47 (6) (2010) 1076–1079.
[35] I. Standard, ISO 13314: 2011 (E)(2011) Mechanical testing of metals—ductility testing—compression test for porous and cellular metals, Ref number ISO 13314(13314) 1-7.
[36] S. Kalidindi, A. Abusafieh, E. El-Danaf, Accurate characterization of machine compliance for simple compression testing, Exp. Mech. 37 (2) (1997) 210–215.
[37] T. Craeghs, S. Clijsters, E. Yasa, F. Bechmann, S. Berumen, J.-P. Kruth, Determination of geometrical factors in Layerwise Laser Melting using optical process monitoring, Opt. Lasers Eng. 49 (12) (2011) 1440–1446.
[38] S.L. Sing, F.E. Wiria, W.Y. Yeong, in: Selective Laser Melting of Lattice Structures: a Statistical Approach to Manufacturability and Mechanical Behavior, 49, Robotics and Computer-Integrated Manufacturing, 2018, pp. 170–180.
[39] L. Liu, P. Kamm, F. García-Moreno, J. Banhart, D. Pasini, Elastic and failure response of imperfect three-dimensional metallic lattices: the role of geometric defects induced by Selective Laser Melting, J. Mech. Phys. Solids 107 (2017) 160–184.
[40] O. Cansizoglu, O. Harrysson, D. Cormier, H. West, T. Mahale, Properties of Ti–6Al–4V non-stochastic lattice structures fabricated via electron beam melting, Mater. Sci. Eng.: A 492 (1–2) (2008) 468–474.
[41] H. Shipley, D. McDonnell, M. Culleton, R. Coull, R. Lupoi, G. O'Donnell, D. Trimble, Optimisation of process parameters to address fundamental challenges during selective laser melting of Ti-6Al-4V: a review, Int. J. Mach. Tools Manuf. 128 (2018) 1–20.
[42] R. Hedayati, S. Janbaz, M. Sadighi, M. Mohammadi-Aghdam, A. Zadpoor, How does tissue regeneration influence the mechanical behavior of additively manufactured porous biomaterials? J. Mech. Behav. Biomed. Mater. 65 (2017) 831–841.
[43] R. Wauthle, B. Vrancken, B. Beynaerts, K. Jorissen, J. Schrooten, J.-P. Kruth, J. Van Humbeeck, Effects of build orientation and heat treatment on the microstructure and mechanical properties of selective laser melted Ti6Al4V lattice structures, Addit. Manuf. 5 (2015) 77–84.
[44] R. Hedayati, S. Ahmadi, K. Lietaert, B. Pouran, Y. Li, H. Weinans, C. Rans, A. Zadpoor, Isolated and modulated effects of topology and material type on the mechanical properties of additively manufactured porous biomaterials, J. Mech. Behav. Biomed. Mater. 79 (2018) 254–263.
[45] M. Ashby, The properties of foams and lattices, Philos. Trans. R. Soc. A: Math. Phys. Eng. Sci. 364 (2006) 15–30.
[46] V. Deshpande, M. Ashby, N. Fleck, Foam topology: bending versus stretching dominated architectures, Acta Mater. 49 (6) (2001) 1035–1040.
[47] A.A. Zadpoor, Mechanics of Additively Manufactured Biomaterials, Elsevier, 2017.
[48] L.J. Gibson, M.F. Ashby, Cellular Solids: Structure and Properties, Cambridge University Press, 1999.
[49] A.A. Zadpoor, R. Hedayati, Analytical relationships for prediction of the mechanical properties of additively manufactured porous biomaterials, J. Biomed. Mater. Res. Part A 104 (12) (2016) 3164–3174.
[50] S. Babaee, B.H. Jahromi, A. Ajdari, H. Nayeb-Hashemi, A. Vaziri, Mechanical properties of open-cell rhombic dodecahedron cellular structures, Acta Mater. 60 (6–7) (2012) 2873–2885.
[51] R. Hedayati, M. Sadighi, M. Mohammadi-Aghdam, H. Hosseini-Toudeshky, Comparison of elastic properties of open-cell metallic biomaterials with different unit cell types, J. Biomed. Mater. Res. Part B: Appl. Biomater. 106 (1) (2018) 386–398.
[52] 3DSystems, LaserForm Ti Gr23 (A) (2018).
[53] R. Hedayati, M. Sadighi, M. Mohammadi-Aghdam, A. Zadpoor, Mechanical behavior of additively manufactured porous biomaterials made from truncated cuboctahedron unit cells, Int. J. Mech. Sci. 106 (2016) 19–38.
[54] A. Acciaioli, G. Lionello, M. Baleani, Experimentally achievable accuracy using a digital image correlation technique in measuring small-magnitude (< 0.1%) homogeneous strain fields, Materials 11 (5) (2018) 751.
[55] L. Xiao, W. Song, Additively-manufactured functionally graded Ti-6Al-4V lattice structures with high strength under static and dynamic loading: experiments, Int. J. Impact Eng. 111 (2018) 255–272.
[56] B. Gorny, T. Niendorf, J. Lackmann, M. Thoene, T. Troester, H. Maier, In situ characterization of the deformation and failure behavior of non-stochastic porous structures processed by selective laser melting, Mater. Sci. Eng.: A 528 (27) (2011) 7962–7967.
[57] T. Niendorf, F. Brenne, M. Schaper, Lattice structures manufactured by SLM: on the effect of geometrical dimensions on microstructure evolution during processing, Metall. Mater. Trans. B 45 (4) (2014) 1181–1185.
[58] H. Kolken, K. Lietaert, T. van der Sloten, B. Pouran, A. Meynen, G. Van Loock, H. Weinans, L. Scheys, A.A. Zadpoor, Mechanical performance of auxetic meta-biomaterials, J. Mech. Behav. Biomed. Mater. 104 (2020) 103658.
[59] K. Genovese, S. Leeflang, A.A. Zadpoor, Microscopic full-field three-dimensional strain measurement during the mechanical testing of additively manufactured porous biomaterials, J. Mech. Behav. Biomed. Mater. 69 (2017) 327–341.
[60] M. Simonelli, Y.Y. Tse, C. Tuck, Effect of the build orientation on the mechanical properties and fracture modes of SLM Ti–6Al–4V, Mater. Sci. Eng.: A 616 (2014) 1–11.
[61] S.A. Goldstein, The Mechanical Properties of Trabecular Bone: Dependence on Anatomic Location and Function, 1987.
[62] P.S. Patel, D.E. Shepherd, D.W. Hukins, Compressive properties of commercially available polyurethane foams as mechanical models for osteoporotic human cancellous bone, BMC Musculoskeletal Disord. 9 (1) (2008) 137.
[63] C. West, J.C. Fryman, Cadaveric Measurement of Impact Force on Total Hip Arthroplasty Surgical Instrumentation, Am Soc Biomech Conference, 2008.
[64] M.J. Nine, D. Choudhury, A.C. Hee, R. Mootanah, N.A.A. Osman, Wear debris characterization and corresponding biological response: artificial hip and knee joints, Materials 7 (2) (2014) 980–1016.
[65] C.M. Bidan, F.M. Wang, J.W. Dunlop, A three-dimensional model for tissue deposition on complex surfaces, Comput. Methods Biomech. Biomed. Eng. 16 (10) (2013) 1056–1070.
[66] G.S. Jung, M.J. Buehler, Multiscale mechanics of triply periodic minimal surfaces of three-dimensional graphene foams, Nano Lett. 18 (8) (2018) 4845–4853.
[67] M. Silva, E.F. Shepherd, W.O. Jackson, F.J. Dorey, T.P. Schmalzried, Average patient walking activity approaches 2 million cycles per year: pedometers underrecord walking activity, J. Arthroplasty 17 (6) (2002) 693–697.
[68] S.A. Yavari, R. Wauthlé, J. van der Stok, A. Riemslag, M. Janssen, M. Mulier, J.-P. Kruth, J. Schrooten, H. Weinans, A.A. Zadpoor, Fatigue behavior of porous biomaterials manufactured using selective laser melting, Mater. Sci. Eng.: C 33 (8) (2013) 4849–4858.
[69] J. de Krijger, C. Rans, B. Van Hooreweder, K. Lietaert, B. Pouran, A.A. Zadpoor, Effects of applied stress ratio on the fatigue behavior of additively manufactured porous biomaterials under compressive loading, J. Mech. Behav. Biomed. Mater. 70 (2017) 7–16.
[70] S. Li, L.E. Murr, X. Cheng, Z. Zhang, Y. Hao, R. Yang, F. Medina, R. Wicker, Compression fatigue behavior of Ti–6Al–4V mesh arrays fabricated by electron beam melting, Acta Mater. 60 (3) (2012) 793–802.
[71] S. Zhao, S. Li, W. Hou, Y. Hao, R. Yang, R. Misra, The influence of cell morphology on the compressive fatigue behavior of Ti-6Al-4V meshes fabricated by electron beam melting, J. Mech. Behav. Biomed. Mater. 59 (2016) 251–264.
[72] S. Ahmadi, R. Hedayati, Y. Li, K. Lietaert, N. Tümer, A. Fatemi, C. Rans, B. Pouran, H. Weinans, A. Zadpoor, Fatigue performance of additively manufactured meta-biomaterials: the effects of topology and material type, Acta Biomater. 65 (2018) 292–304.
[73] A.A. Zadpoor, Mechanical performance of additively manufactured meta-biomaterials, Acta Biomater. 85 (2019) 41–59.